



NUMERICAL SIMULATION OF DROPLET IMPACT AND SOLIDIFICATION INCLUDING THERMAL SHRINKAGE IN A THERMAL SPRAY PROCESS

Sina Alavi and Mohammad Passandideh-Fard*

Department of Mechanical Engineering, Ferdowsi University of Mashhad, Mashhad, Iran

ABSTRACT

In this paper, a numerical study is performed to investigate the effects of thermal shrinkage on the deposition of molten particles on a substrate in a thermal spray process using the Volume-of-Fluid (VOF) method. Thermal shrinkage is a phenomenon caused by the variation of density during cooling and solidification of a molten metal. The Navier-Stokes equations along with the energy equation including phase change are solved using a 2D/axisymmetric mesh. The VOF method is used to track the free surface of molten particles, and an enthalpy-porosity formulation is used to model solidification. For the normal impact of tin particles in the order of 2 mm in diameter and 1 m/s in impact velocity, the final splat had a single cavity inside due to shrinkage. For cases with the scales of a typical thermal spray process, the effect of shrinkage appeared as a reduction in the droplet splashing on the substrate.

Keywords: *Thermal shrinkage, Thermal spray coating, VOF method, Solidification, Molten metal droplets*

1. INTRODUCTION

In thermal spray processes, coatings such as various metals and alloys, carbides, and ceramics are applied to metal surfaces by a spray gun with a stream of oxyfuel flame, electric arc, or plasma arc. These coatings are formed by spraying and deposition of molten droplets on the substrate. The properties and quality of these coatings depend on many factors such as flame/laser/arc, material used for spraying, substrate material and its surface conditions, and spray characteristics.

Another phenomenon that affects the shape of droplets in thermal spraying is thermal shrinkage. Because of their thermal expansion characteristics and changes in density, metals shrink or contract during solidification and cooling. Shrinkage, which causes dimensional changes and sometimes cracking, is the result of these three phases:

- Contraction of a molten metal as it cools prior to its solidification.
- Contraction of the metal during phase change from liquid to solid (release of the latent heat of fusion).
- Contraction of the solidified metal (casting) as its temperature drops to the ambient temperature.

The shrinkage occurs because in most of the materials, the volume decreases due to an increase in density when the material

undergoes solidification and cooling. Shrinkage can cause various defects in manufacturing processes. These defects can affect the appearance or even the structural integrity of the final product. Some examples are cavities, porosities, discontinuities such as cracks, defective surface, etc. In a thermal spray process, shrinkage has some effects on the deposition of droplets on the substrate and the formation of coating including porosity, cavity, curl-up of splat and surface depression.

Developing a model to simulate impacts and solidification of molten droplets on to a substrate is a complex problem. It involves simultaneous computing of heat transfer and fluid flow in a droplet with a moving free surface. Adding phase change and density variation in this phenomenon makes the problem more complex. Modeling droplet impacts has a long history. Harlow and Shannon (1967) were the first to simulate the impact of droplets. Later, Tsurutani *et al.* (1990) and Trapaga and Szekely (1991) studied the impact of molten droplets in thermal spray processes. More studies were done by Sicilian and Hirt (1988), Kothe *et al.* (1991), Brackbill *et al.* (1992), Pasandideh-Fard *et al.* (1996 & 1998), Zhao *et al.* (1996), Fukai *et al.* (1995), Bertagnoli *et al.* (1997), and Waldvogel and Poulidakos (1997). Moreover, Bussmann *et al.* (1999 & 2000) developed a 3D model to simulate water droplet impacts and Pasandideh-Fard *et al.* (2002) extended it to study metal droplet impacts. A level set method was also developed by Zheng and Zhang (2000) to study droplet impact and phase change with no shrinkage.

To model shrinkage during solidification, Trovant and Argyropoulos (1996) developed a numerical model for cylindrical casting of aluminum and magnesium based on a fixed-grid 2D

* Corresponding author, Associate Professor, Email: mpfard@um.ac.ir

axisymmetric mesh. A similar model was presented by Beech *et al.* (1998) to compute solidification shrinkage in cylindrical and T-shaped castings using the Flow-3D software (Barkhudarov, 1995). Also, Kim and Ro (1993) had a similar study on the occurrence of solidification shrinkage in a 2D rectangular mold. All algorithms mentioned above, are suitable for cases in which the liquid is quiescent and the geometry is simple. Therefore, MacBride *et al.* (1999) presented a 2D model to account for directional solidification in dendritic binary alloys which includes the effect of shrinkage-induced flow. Similarly, Chiang and Tsai (1992) analyzed fluid flow and domain change caused by solidification shrinkage in a 2D rectangular cavity filled with molten alloys. Finally, using a 2D finite volume model based on the volume averaging, Ehlen *et al.* (2000) predicted the transient shape of the melt surface, the shrinkage cavity locations, and their influence on the final solute distribution of AlSi alloy. Moreover, to apply the Volume-of-Fluid (VOF) method to the cases where the density is not constant, they modified the classic donor-acceptor flux approximation. Finally, Raessi and Mostaghimi (2005) modified the model used by Pasandideh-Fard *et al.* (2002) to account for density variation and modeled shrinkage in solidification of metal droplet impacts. However, in their model, the governing equations are derived under the assumption that densities in solid and liquid phases are different but constant.

The effect of shrinkage on the formation of coating in a thermal spray process has received little attention. In the literature, however, more studies for investigating this effect on other applications are available. Hou *et al.* (2008) developed a new method called EIECAM to predict the shrinkage defects formed in casting of ductile iron. Cai *et al.* (2011) used a thermal-mechanical coupled model in the ANSYS software to study the influence of shrinkage in solidification of four round billets within four different shapes of molds. Using the simulation, they obtained an optimum shape of mold to be used in continuous casting of round steel billets. Moreover Nandi *et al.* (2011) used the VEM-based casting simulation software to study the behavior of solidification in chunky castings. They included shrinkage in molds with different dimensions of riser neck and determined optimum neck sizes for which the shrinkage in the castings can be eliminated.

In this paper, we study numerically the effects of shrinkage and density variation in solidification of molten tin and nickel droplets while they impact and spread on cold substrates. The novelty of this study is that the material density is assumed to vary with temperature in both the liquid and solid phases as well as during solidification. The Fluent commercial software is used to perform the simulations. The effects of shrinkage on the splat shape and porosity formation are investigated in various scenarios.

2. NUMERICAL METHOD

2.1 Fluid Flow

In this paper, the fluid flow of the impacting droplet is modeled using a finite-volume method. The momentum equations are solved in an axisymmetric coordinate system. The liquid, in this case a molten metal, is modeled as an incompressible fluid. The fluid flow can be assumed laminar because the Reynolds number, considering the flow over a flat plate, is at most in the order of 10^4 . The continuity and Navier-Stokes equations are as follows:

$$\nabla \cdot \mathbf{V} = 0 \quad (1)$$

$$\frac{\partial}{\partial t}(\rho \mathbf{V}) + \nabla \cdot (\rho \mathbf{V} \mathbf{V}) = -\nabla P + \nabla \cdot (\mu \nabla \mathbf{V}) + \mathbf{g} + \mathbf{S} \quad (2)$$

In these equations, ρ is the density, P pressure, μ viscosity, \mathbf{g} gravitational acceleration, and \mathbf{V} is the fluid velocity. \mathbf{S} is a source term that will be defined in the next section.

Using the VOF technique applied to a fixed Eulerian mesh, the free surface of the droplet is tracked. In this technique, a scalar function f is defined. This function shows the fraction of a cell filled with liquid. When a cell is fully occupied by liquid, it is set to unity and consequently when a cell is empty of liquid, f equals to zero. In other cases f is between zero and one. For surface tension we used the continuum surface force (CSF) model integrated with smoothed values of function f in evaluating free surface curvature. Surface tension and contact angle are assumed to be constant but thermal conduction and especially density are taken to vary with temperature. Further details of fluid flow simulations can be seen elsewhere (Bussmann *et al.*, 1999; Pasandideh-Fard *et al.*, 2002). The properties of tin and nickel for the droplets and of air are taken from the published literature (Incropera and DeWitt, 2007; Raessi and Mostaghimi, 2005; and Stankus and Khairulin, 2006).

2.2 Heat Transfer and Solidification

Many efforts have been put into modeling the moving boundary problems including solidification in fixed grid analyses. The problem that arises is how to deal with the velocity in the mushy and completely-solidified regions. Here, we employ the method introduced by Voller and Prakash (1987) which considers the solidification mushy zone as a pseudo-porous medium. In this method, the Darcy source approach is used to model the motion in mushy zones.

To begin, the total enthalpy in the droplet is introduced as the sum of sensible heat h and latent heat ΔH as follows:

$$H = h + \Delta H \quad (3)$$

where

$$h = h_{ref} + \int_{T_{ref}}^T c_p dT \quad (4)$$

where h_{ref} and T_{ref} are the reference sensible heat and temperature, respectively, and c_p is the specific heat at constant pressure.

As mentioned, for the solidification, we used an enthalpy-porosity technique in which the liquid-solid front is not tracked explicitly. Instead, a quantity named liquid/solid fraction β (different from f) is used in every cell based on following relations:

$$\begin{aligned} \beta &= 0 & \text{if } T < T_{solidus} \\ \beta &= \frac{T - T_{solidus}}{T_{liquidus} - T_{solidus}} & \text{if } T_{solidus} < T < T_{liquidus} \\ \beta &= 1 & \text{if } T > T_{liquidus} \end{aligned} \quad (5)$$

In fact, the liquid/solid fraction shows the fraction of every cell which is filled with liquid material (molten metal). The second term in the previous relation represents a zone which is called the solidification mushy zone. In this zone, the liquid/solid fraction is between zero and one. As the material solidifies in a cell, β reduces from one to zero. By definition of the liquid/solid fraction, we can now write the latent heat content in terms of the latent heat of material:

$$\Delta H = \beta L \quad (6)$$

where L is the latent heat of material and ΔH can vary between zero for solid and L for liquid.

The energy equation for solidification/melting problems can now be written as:

$$\frac{\partial}{\partial t}(\rho H) + \nabla \cdot (\rho \mathbf{V} H) = \nabla \cdot (k \nabla T) \quad (7)$$

in which H should be substituted from Eq. 3. As mentioned above, the mushy zone is modeled using a liquid/solid fraction β . When β reduces during solidification in a cell, velocity drops to zero. This procedure is accomplished using the source term S to modify the momentum equation (Eq. 2). For this purpose, we assume that the flow of material in the mushy zone is governed by the Darcy law (Voller and Prakash, 1987):

$$\mathbf{V} = -(\kappa / \mu) \nabla P \quad (8)$$

where $\kappa(\beta)$ is the permeability factor (not to be confused with conductivity k). Moreover, the source term in Eq. 2 is defined as:

$$S = \frac{(1-\beta)^2}{(\beta^3 + \varepsilon)} A_{mush} (\mathbf{V} - \mathbf{V}_p) \quad (9)$$

where ε is a small number to prevent division by zero. \mathbf{V}_p is the pull velocity set to zero in this study because the solidified material is not pulled out of the domain (like in continuous casting processes).

The coefficient of $(\mathbf{V} - \mathbf{V}_p)$ in Eq. 9, increases from zero for liquid to a large value as the material solidifies. Consequently, as the liquid solidifies, the effect of source term S becomes more dominant against all other terms in the momentum equation (which results in the Darcy law) and; therefore, the velocity approaches zero for the solid regions. A_{mush} is the mushy zone constant and specifies the slope at which velocity drops to zero as the material solidifies. Increasing this constant makes the slope steeper. In this paper, this constant was set to 10^9 . This method, facilitates the modification of velocity in solid regions and can be used both for a pure material (for which solidification occurs in a certain temperature) and for an alloy (which includes mushy zone between $T_{solidus}$ and $T_{liquidus}$). It should be mentioned that there is no mushy zone for a pure metal. In the numerical model, however, the discontinuity of density at the melting point causes a divergence problem. Therefore, in the case of pure tin, it is assumed that the density changes linearly with temperature as the solidification occurs. In the simulations for nickel, one of its alloys is used; as a result, mushy zone in this case is physical.

2.3 Shrinkage

The material shrinkage is characterized by the shrinkage factor defined as:

$$\text{Shrinkage factor} = \frac{\rho_s - \rho_l}{\rho_l} \quad (10)$$

where ρ_l and ρ_s are the densities of liquid and solid phases, respectively. Table 1 shows the amount of shrinkage factor for some metals/alloys.

TABLE 1 Shrinkage factor for some metals/alloys (Kalpakjian, 1989)

Metal/Alloy	Shrinkage Factor (%)
Aluminum	6.6
Carbon Steel	2.5 – 3
White Iron	4 – 5.5
Tin	3.3
Nickel	2.8

For tin and nickel which are of interest in this study, the density variation with temperature is displayed in Fig. 1 and 2 (the data used in plotting Fig. 1 are those reported by Stankus and Khairulin, 2006). As shown in these figures, density decreases with increasing temperature.

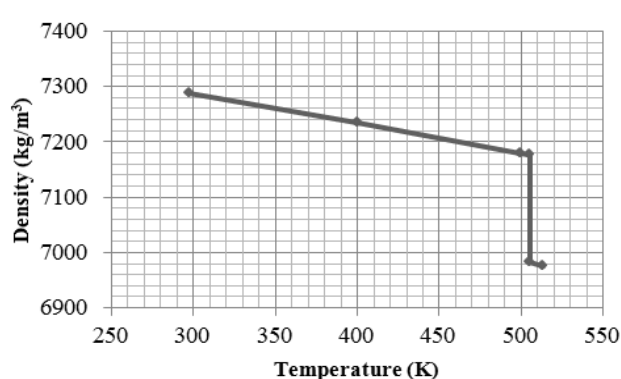


Fig. 1 Density variation of tin vs. temperature (the data used are those reported by Stankus and Khairulin, 2006)

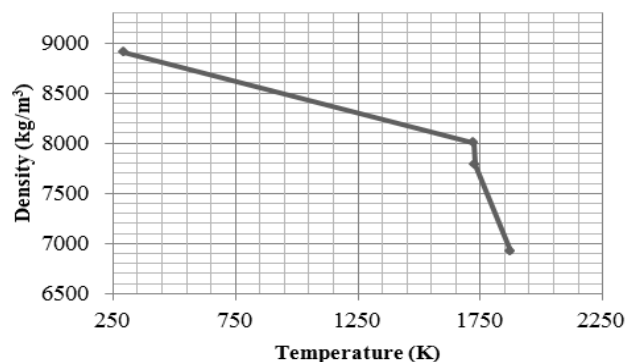


Fig. 2 Density variation of nickel vs. temperature

Tin droplets are at 240°C (513K) when they impinge on the substrate which is at 27°C (300K). Using the data for tin density and the relation for shrinkage factor, its value for the droplet in this process would be 4.42%. This amount involves liquid phase, solidification and solid phase shrinkage. Also for nickel droplets with an initial temperature of 1600°C (1873K) and a substrate temperature of 400°C (673K), the shrinkage factor would be 25.3% (in comparison with tin, in this process, the nickel temperature varies from 1873K to 673K and this is why the shrinkage factor for nickel is more pronounced than that of tin). Simulations based on the above-mentioned numerical method were performed using the Fluent commercial software. The typical mesh size used for the simulation consisted of 50 cpr (cell per radius of the droplet). A typical CPU time was in the order of 5 hrs.

3. RESULTS AND DISCUSSION

Tin properties are listed in Table 2. Thermal conductivity and density are assumed to change linearly with temperature to avoid any divergences caused by the discontinuity of density when solidification occurs. Tin droplets impinge at a temperature of 513K onto the substrate which is at 300K. A thermal contact resistance is considered between the droplet and the substrate. This resistance is estimated to be approximately $5 \times 10^{-6} \text{ m}^2\text{K/W}$ (Pasandideh-Fard *et al.*, 1996). It should be indicated that in an actual thermal spray coating process, the contact resistance between droplets and substrate is not constant. This value varies from the center of a splat toward the peripheral regions. Several simulations were performed to find the optimum boundary condition for the substrate. The results of the simulation assuming a constant-temperature wall with a constant thermal contact resistance were found to be in a better agreement with those of the available experiments. Therefore, for simulations

performed in this paper, the substrate is considered as a wall with constant temperature and contact resistance.

Figure 3 shows the results for a 2D axisymmetric analysis. The droplet impacts with a velocity of 1m/s normal to the substrate. Before the impact, it is assumed that the droplet has the shape of a sphere with a diameter of 2.7mm. The values of the initial conditions for the droplet are the same as those available in the literature (Raessi and Mostaghimi, 2005). The left half of each image in the figure belongs to the case with shrinkage and the right half to the constant density. As the droplet impacts, it begins to spread on the substrate and since the temperature of the substrate is less than that of the droplet, it solidifies and deposits on the substrate. At $t = 4.5\text{ms}$, the droplet reaches its maximum spread on the surface since the effects of surface tension forces overcome the effects of inertial forces. At this time, the droplet is like a flattened disk with raised rims and the

part of the droplet in contact with the cold substrate is solidified. After this time, the effects of surface tension forces cause the remaining molten part of the droplet to recoil on the solidified layer and form a recoiling ring. This ring meets at the center of the droplet and, as a result, a void is formed at the center of the deposited droplet. Close inspection of the numerical results reveals that this void is caused by shrinkage, i.e., no cavity is seen to form in the right half of the images shown in Fig. 3. The recoiled molten tin reaches a maximum height between 8.3ms and 11.3ms (approximately at $t=10\text{ms}$) elapsed after the impact. Capillary effects cause necking in the molten column. This phenomenon can be seen in the results shown in Fig. 3.

Later, the melt column falls down under the effects of gravity and surface tension. Finally, after the entire molten tin is solidified, a splat remains on the substrate.

TABLE 2 Properties of tin in solid and liquid phases (Stankus and Khairulin, 2006)

Phase	Density (kg/m ³)	Thermal conductivity (W/m K)	Specific Heat (J/kg K)	Kinematic viscosity (m ² /s)	Surface tension (N/m)	Latent heat (kJ/kg)	Melting point (K)
Solid	-1.491T+7733	-0.154T+113.0	244	-	-	60.9	505
Liquid	(T in Kelvins)	(T in Kelvins)	243	2.7×10^{-7}	0.526		

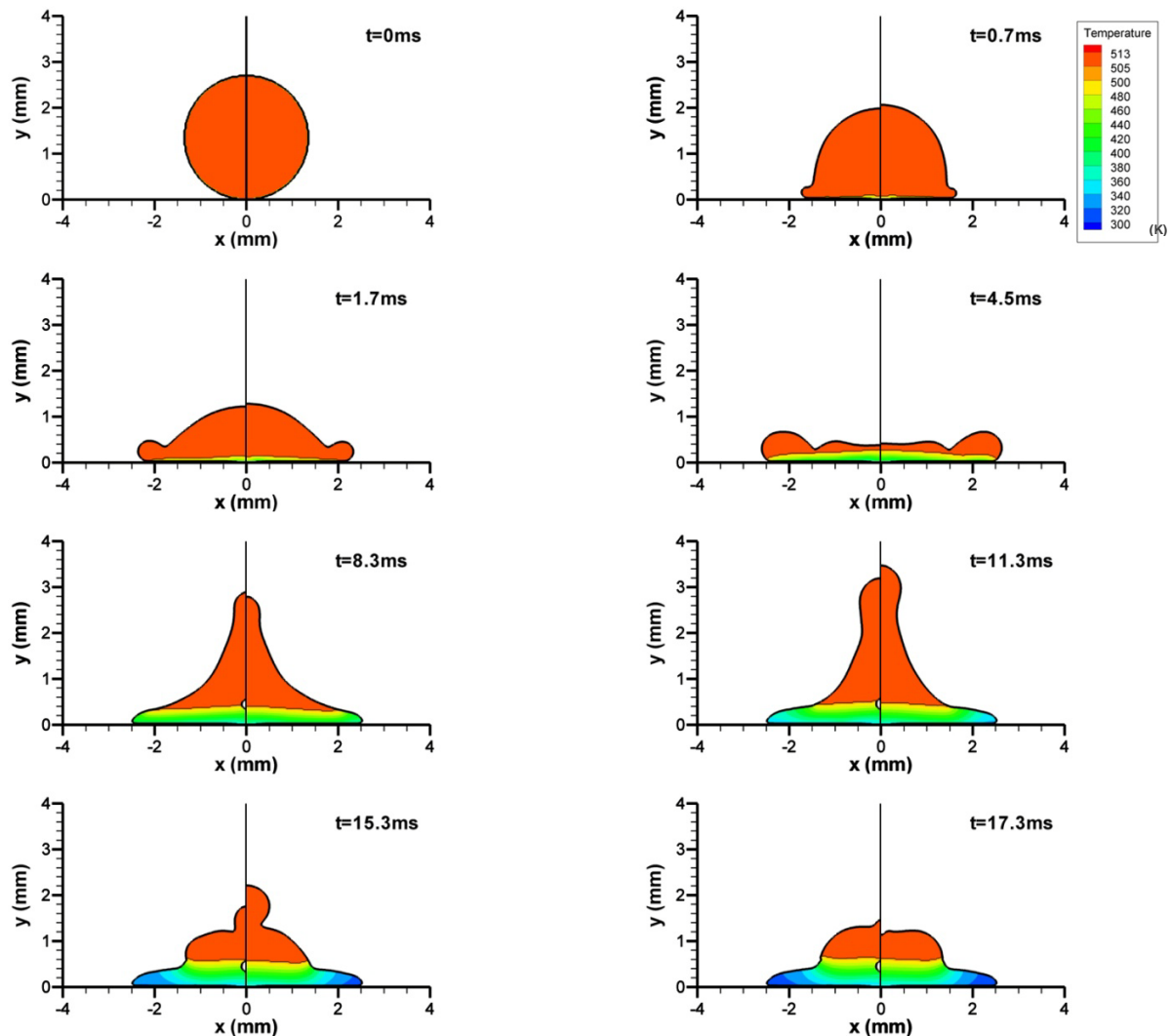


Fig. 3 Temperature distribution in a 2.7mm dia. tin droplet impacting at 240°C (513K) with a velocity of 1m/s onto a substrate with a constant temperature of 27°C (300K). The left half of each image corresponds to the case with variable density (i.e. with shrinkage) and the right half to the constant density. Solidification front is seen as a black line inside the droplet.

Figure 3 also shows the calculated temperature distribution in droplets. It is clear from this figure that as the droplet makes its first contact with the substrate, the drop begins to lose heat through the wall. In this study, the effects of ambient air on the droplet and heat transfer between air and droplet is taken into account. In displaying the figure, however, the temperature distribution inside air is not shown because the droplet domain is of interest in this study.

It can be seen in Fig. 3 that in the peripheral regions of the splat where the thickness is smaller (i.e. the thermal resistance is smaller) the temperature drops faster than in the central regions. Also, shrinkage in these regions slightly reduces the maximum amount of spread on the substrate.

Figure 4 shows the impact of tin droplets with the same conditions as those of Fig. 3 except for the impact velocity which was increased to 2 m/s. In comparison with Fig. 3 in which the initial velocity was 1 m/s, the droplet spreads more on the surface and the thickness of the deposited droplet is lower than in the previous case. This in turn causes the droplet to solidify and to cool down much

faster. Because of this initial velocity, the droplet does not recoil and, as a result, there would be no void in the center of the final solidified splat in contrast to what is seen in the case of 1 m/s (Fig. 3).

Therefore, the effect of shrinkage in forming macroporosities is reduced by a higher impact velocity. Although the effects of shrinkage are not clear in the first three images of Fig. 4, the difference between the variable and constant density cases can be seen in the last image ($t = 21.02\text{ms}$) where the droplet is completely solidified. It can be seen that the surface of the droplet is further depressed when shrinkage factor is considered. The image shows that the splat surface for the left half related to the case with variable density is lower than that of the right half with constant density.

The next cases considered are those of a typical thermal spray process for nickel particles. For nickel, we assumed density to be piecewise linear; it can be seen in Fig. 2 that this assumption is acceptable. Density and other properties are listed in Table 3. Note that the thermal conductivity and specific heat are assumed to be constant.

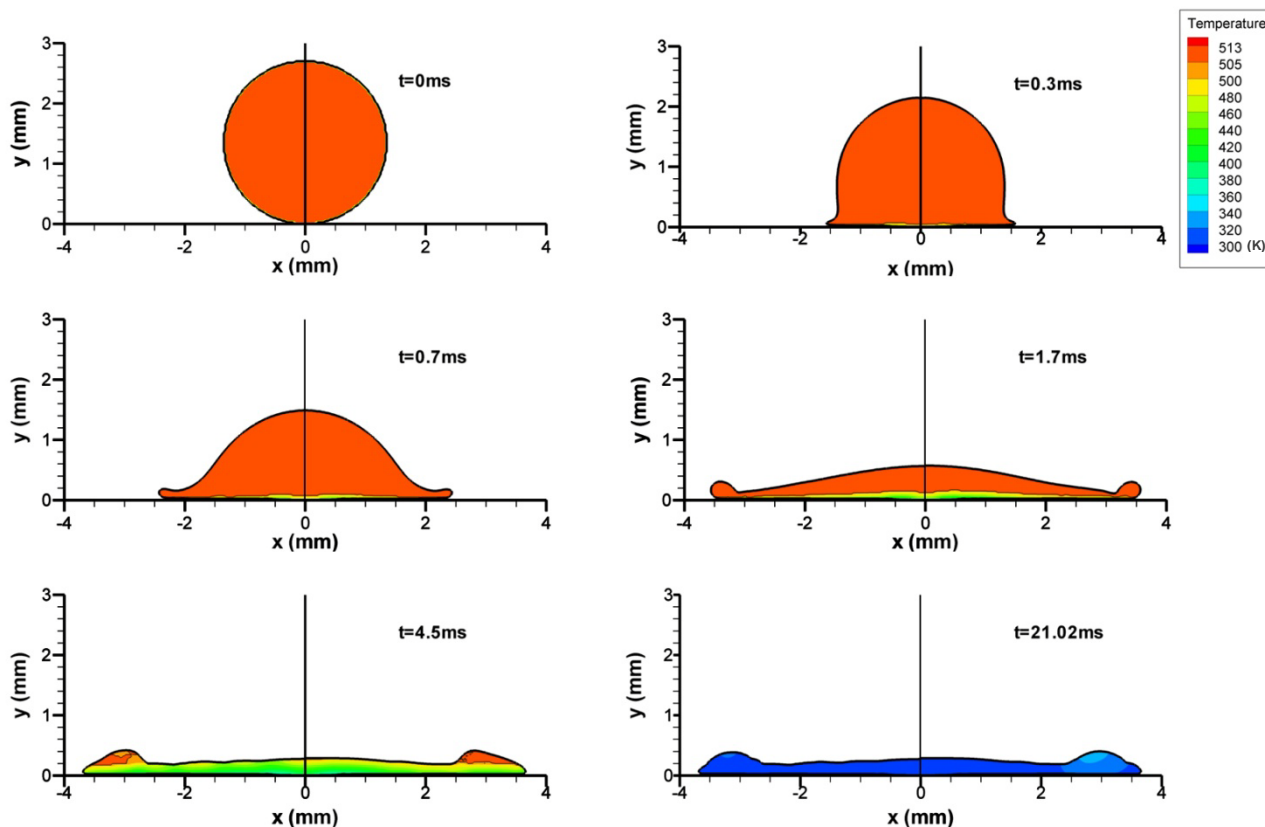


Fig. 4 Temperature distribution in a 2.7mm dia. tin droplet impacting at 240°C (513K) with a velocity of 2m/s onto a substrate with a constant temperature of 27°C (300K). The left half of each image corresponds to the case with variable density (i.e. with shrinkage) and the right half to the constant density. Solidification front is seen as a black line inside the droplet.

TABLE 3 Properties of nickel in solid and liquid phases

Phase	Density (kg/m ³)	Thermal conductivity (W/m K)	Specific Heat (J/kg K)	Kinematic viscosity (m ² /s)	Latent heat (kJ/kg)	Melting point (K)
Solid	-0.631T+9089 (300 < T < 1723.85)	76.2	600	-	297	1731.85
Mushy zone	-27.66T+55696 (1723.85 < T < 1731.85)					
Liquid	-6.134T+18404 (1731.85 < T < 1873) (T in Kelvins)					

Figure 5 shows the results for the normal impact of a nickel droplet with an initial velocity of 73m/s and a temperature of 1600°C (1873K). The temperature of the substrate in this case is 290°C (563K) and a thermal contact resistance value of 10^{-7} m²K/W is considered between the droplet and substrate (Pasandideh-Fard *et al.*, 2002). Prior to impact, the droplet is assumed to have the shape of a sphere with a diameter of 60µm.

After the impact, parts of the droplet in contact with substrate solidify and the remaining molten nickel will flow over the solidified

regions because of the high impact velocity of the droplet (at $t=1.5\mu\text{s}$). This causes some of the molten material to separate from the solidified splat as a ring and form a splash on the substrate (at $t=6\mu\text{s}$) for the case with no shrinkage (right half of images in Fig. 5). It is seen that shrinkage affects the droplet deposition on the substrate in a way that less splashing occurs and most of the material remains intact. That is, the left side of the images in Fig. 5 shows no liquid breakup and splashing.

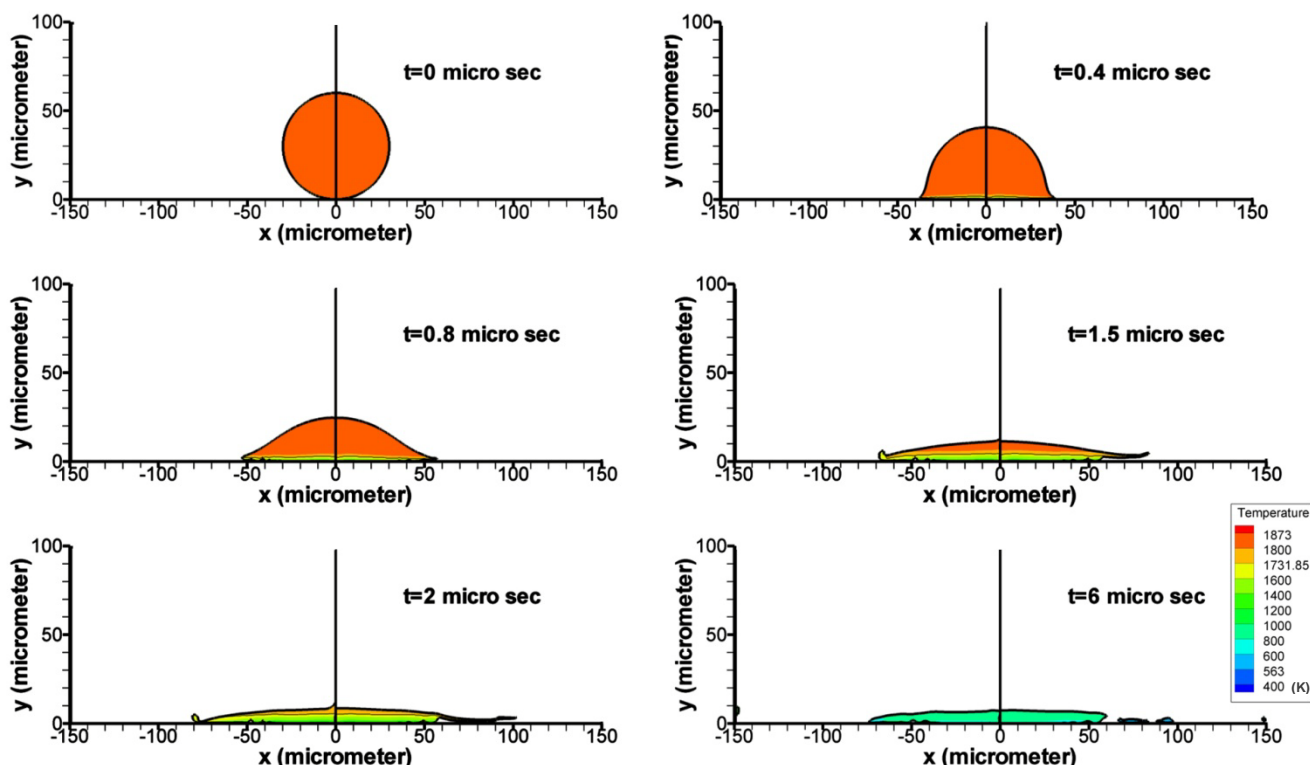


Fig. 5 Temperature distribution in a 60µm dia. nickel droplet impacting at 1600°C (1873K) with a velocity of 73m/s onto a substrate with a constant temperature of 290°C (563K) and a thermal contact resistance of 10^{-7} m²K/W. The left half of each image corresponds to the case with variable density (i.e. with shrinkage) and the right half to the constant density. Solidification front is seen as a black line inside the droplet.

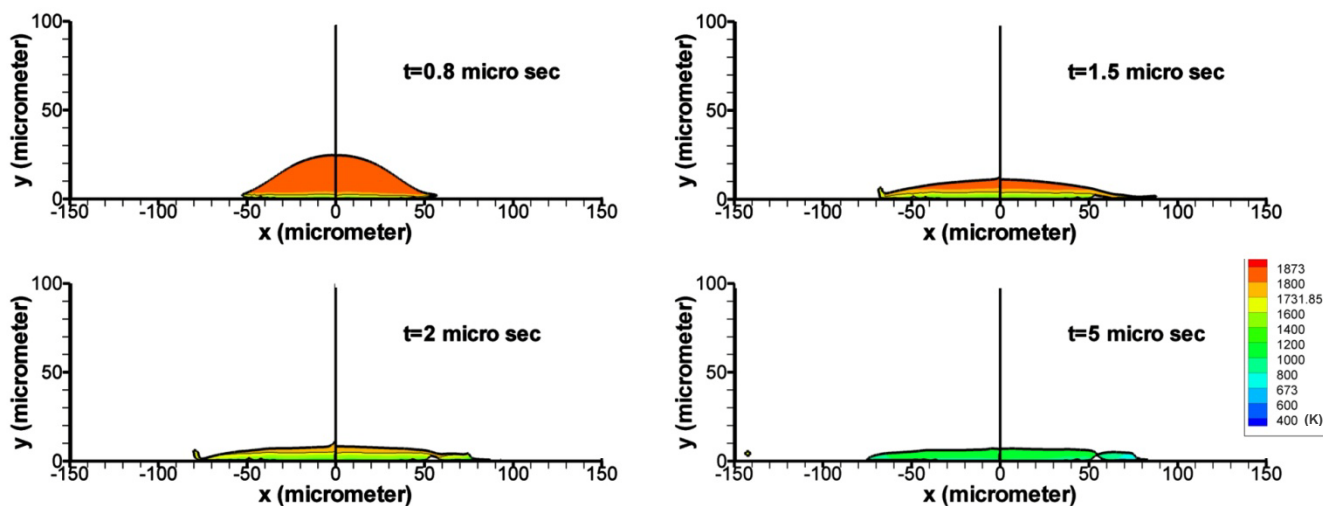


Fig. 6 Temperature distribution in a 60µm dia. nickel droplet impacting at 1600°C (1873K) with a velocity of 73m/s onto a substrate with a constant temperature of 400°C (673K) and a thermal contact resistance of 10^{-7} m²K/W. The left half of each image corresponds to the case with variable density (i.e. with shrinkage) and the right half to the constant density. Solidification front is seen as a black line inside the droplet.

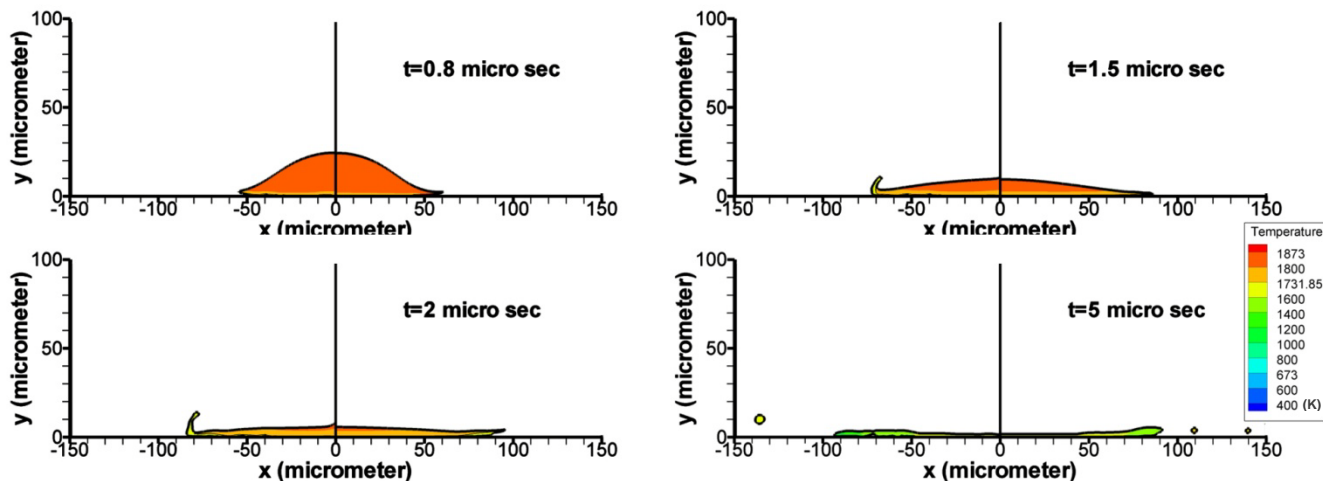


Fig. 7 Temperature distribution in a 60µm dia. nickel droplet impacting at 1600°C (1873K) with a velocity of 73m/s onto a substrate with a constant temperature of 400°C (673K) and a thermal contact resistance of 10^{-6} m²K/W. The left half of each image corresponds to the case with variable density (i.e. with shrinkage) and the right half to the constant density. Solidification front is seen as a black line inside the droplet.

In Fig. 6 and 7, the effects of substrate temperature and contact resistance on droplet impact are displayed, respectively. Figure 6 shows the impact of a nickel droplet onto the substrate which in this case is at 400°C (673K). It can be seen that in comparison with the previous case, in which the temperature of the substrate was 290°C (563K), less splashing occurs during the solidification and deposition of the droplet. However, the effects of shrinkage are still observed as reducing the droplet breakup and splashing.

Finally, to study the effect of contact resistance, we set its value to 10^{-6} m²K/W. Results are shown in Fig. 7. As the figure shows, in this case with a higher contact resistance, the solidification rate decreases and, as a result, the droplet spreads more on the substrate and the thickness of the splat decreases as well. A close inspection of the results revealed that less molten material splashes in comparison with the two previous cases and the differences between the droplets with constant and variable density are less significant. According to reported experiments in the literature, splats in this case are more similar to splats deposited on the substrate in typical spraying processes (Pasandideh-Fard *et al.*, 2002).

4. CONCLUSION

A numerical study was presented on the effects of thermal shrinkage on the deposition and formation of porosity during the impact of molten tin and nickel droplets on a cold substrate. The Navier-Stokes equations were solved using a finite-volume method for a 2D axisymmetric mesh. The VOF model was used to track the free surface of the droplet as it spreads on the substrate. The solidification and density variation which leads to thermal shrinkage were accounted for in this study. The simulations, performed using the Fluent commercial code, included two scenarios for tin particles where 2.7 mm droplets of 1m/s and 2m/s with a temperature of 240°C (513K) impacted normally on to a 27°C (300K) substrate, and three scenarios for nickel particles with high speed micron sized droplets in which the effects of shrinkage, substrate temperature and thermal contact resistance on splats deposition were investigated. Nickel droplets 60µm in diameter with an initial velocity of 73m/s were considered for this purpose.

For tin particles, as the droplet spread on the substrate and recoiled, a small cavity remained in the center of the solidified splat. This cavity was attributed to the shrinkage factor as no cavity was

observed when the density was assumed constant. Increasing the droplet impact speed increased the amount of droplet spread on the substrate, which in turn, reduced the chance of cavity formation inside the splat.

For typical thermal spray coating scenarios with nickel particles, it was found that the material shrinkage decreased the amount of splashing. Increasing the contact resistance and substrate temperature had a similar effect on the droplet deposition on the substrate.

NOMENCLATURE

A_{mush}	mushy zone constant
H	total enthalpy
L	latent heat
P	pressure
S	source term in the Navier-Stokes equations
S_h	source term in the energy equation
T	temperature
T_{ref}	reference temperature
C_p	specific heat
f	volume-of-fluid function
g	gravitational acceleration
h	sensible heat
h_{ref}	reference enthalpy
k	thermal conductivity
t	time
V	velocity
V_p	pull velocity

Greek Symbols

β	liquid/solid fraction
κ	permeability
μ	viscosity
ρ	density

Subscripts

l	liquid
s	solid

REFERENCES

- Barkhudarov, M. R. (1995). "Enhancement to heat transfer and solidification shrinkage models in Flow-3D," *Flow Science, Inc., Rep FSI-95-TN43*.
- Beech, J., Barkhudarov, M., Chang, K., and Chin, S. B. (1998). "Computer modeling of the formation of macro shrinkage cavities during solidification, in B. G. Thomas and C. Beckermann (eds.)," *Proc. Eighth Int. Conf. on Modeling of Casting, Welding and Advanced Solidification Processes*, (pp. 1071-1078). San Diego, CA.
- Bertagnolli, M., Marchese, M., Jacucci, G., St Doltsinis, I., and Noelting, S. (1997). "Thermo-mechanical simulation of the splashing of ceramic droplets on a rigid substrate," *J. Comput. Phys.* **133**, p 205.
[doi:10.1006/jcph.1996.5468](https://doi.org/10.1006/jcph.1996.5468)
- Brackbill, J. U., Kothe, D. B., and Zemach, C. (1992). "A continuum method for modelling surface tension," *J. Comput. Phys.* **100**, pp. 335-354.
[doi:10.1016/0021-9991\(92\)90240-Y](https://doi.org/10.1016/0021-9991(92)90240-Y)
- Bussmann, M., Mostaghimi, J. and Chandra, S. (1999). "On a three-dimensional volume tracking model of droplet impact," *Physics Fluids* **11**, pp. 1406-1417.
[doi:10.1063/1.870005](https://doi.org/10.1063/1.870005)
- Bussmann, M., Chandra, S., and Mostaghimi, J. (2000). "Modeling the splash of a droplet impacting a solid surface," *Phys. Fluids* **12**, pp. 3121-3132.
[doi:10.1063/1.1321258](https://doi.org/10.1063/1.1321258)
- Cai, S. W., Wang, T. M., Xu, J. J., Li, J., Cao, Z. Q., and Li, T. J. (2011). "Continuous casting novel mould for round steel billet optimised by solidification shrinkage simulation," *Material Research Innovation* **15**, pp. 29-35.
[doi:10.1179/143307511X12922272563707](https://doi.org/10.1179/143307511X12922272563707)
- Chiang, K. C., and Tsai, H. L. (1992). "Shrinkage-induced fluid flow and domain change in two-dimensional alloy solidification," *Int. J. Heat Transfer*, **35** (7), pp. 1763-1770.
[doi:10.1016/0017-9310\(92\)90146-J](https://doi.org/10.1016/0017-9310(92)90146-J)
- Ehlen, G., Schweizer, A., Ludwig, A., and Sahn, P. R. (2000). "Free surface model to predict the influence of shrinkage cavities on the solute redistribution in castings, in P. R. Sahn, P. N. Hansen and J. G. Conley (eds.)," *Proc. Ninth Int. Conf. on Modeling of Casting, Welding and Advanced Solidification Processes*, (p. 632). Aachen, Germany.
- Fukai, J., Shiiba, Y., Yamamoto, T., Miyatake, O., Poulikakos, D., Megaridis, C.M., and Zhao, Z. (1995). "Wetting effects on the spreading of a liquid droplet colliding with a flat surface: experiment and modeling," *Phys. Fluids* **7**, pp. 236-247.
[doi:10.1063/1.868622](https://doi.org/10.1063/1.868622)
- Harlow, F. H., and Shannon, J. P. (1967). "The splash of a liquid droplet," *J. Appl. Phys.* **38**, p 3855.
[doi:10.1063/1.1709031](https://doi.org/10.1063/1.1709031)
- Hirt, C. W., and Nicholas, B. D. (1981). "Volume of fluid (VOF) methods for the dynamics of free boundaries," *J. Comput. Phys.* **39**, pp. 201-225.
[doi:10.1016/0021-9991\(81\)90145-5](https://doi.org/10.1016/0021-9991(81)90145-5)
- Hou, H., Zhang, G. W., Mao, H. K., and Cheng, J. (2008). "A new prediction way to shrinkage cavity formation for ductile iron castings," *Material Science Forum* **575-578**, pp. 127-134.
[doi:10.4028/www.scientific.net/MSF.575-578.127](https://doi.org/10.4028/www.scientific.net/MSF.575-578.127)
- Incropera, F. P., DeWitt, D. P., Gergman T. L., and Lavine, A. S. (2007). *Introduction to Heat Transfer, fifth ed.* John Wiley and Sons, New York.
- Kalpakjian, S. (1989). *Manufacturing Engineering and Technology, Third Edition.* Addison-Wesley Publishing Company.
- Kim, C. J., and Ro, S. T. (1993). "Shrinkage formation during the solidification process in an open rectangular cavity," *ASME J. Heat Transfer*, **115**, pp. 1078-1081.
[doi:10.1115/1.2911369](https://doi.org/10.1115/1.2911369)
- Kothe, D. B., Mjolsness, R. C., and Torrey, M. D. (1991). "RIPPLE: a computer program for incompressible flows with free surfaces," Technical Report LA-12007-MS, LANL. Los Alamos, NM.
- McBride, E., Heinrich, J. C., and Poirier, D. R. (1999). "Numerical simulation of incompressible flow driven by density variation during phase change," *Int. J. Numer. Meth. Fluids*, **31**, pp. 787-800.
[doi:10.1002/\(SICI\)1097-0363\(19991115\)31:5<787::AID-FLD973>3.0.CO;2-W](https://doi.org/10.1002/(SICI)1097-0363(19991115)31:5<787::AID-FLD973>3.0.CO;2-W)
- Nandi, T., Behera, R., Chandra, A., and Sutradhar, G. (2011). "Study on solidification behaviour of LM6 castings by using computer-aided simulation software," *Indian Foundry Journal* **57**, pp. 44-49.
- Pasandideh-Fard, M., Qiao, Y. M., Chandra, S., and Mostaghimi, J. (1996). "Capillary effects during droplet impact on a solid surface," *Phys. Fluids* **8**, pp. 650-659.
[doi:10.1063/1.868850](https://doi.org/10.1063/1.868850)
- Pasandideh-Fard, M., Bhola, R., Chandra, S., and Mostaghimi, J. (1998). "Deposition of tin droplets on a steel plate: simulations and experiments," *Int. J. Heat Mass Transfer* **41**, pp. 2929-2945.
[doi:10.1016/S0017-9310\(98\)00023-4](https://doi.org/10.1016/S0017-9310(98)00023-4)
- Pasandideh-Fard, M., Chandra, S. and Mostaghimi, J. (2002). "A three-dimensional model of droplet impact and solidification," *Int. J. Heat Mass Transfer* **45**, pp. 2229-2242.
[doi:10.1016/S0017-9310\(01\)00336-2](https://doi.org/10.1016/S0017-9310(01)00336-2)
- Pasandideh-Fard, M., Pershin, V., Chandra, S., and Mostaghimi, J. (2002). "Splat shapes in a thermal spray coating process: simulation and experiments," *J. Thermal Spray Technol.*, (in press).
[doi:10.1361/105996302770348862](https://doi.org/10.1361/105996302770348862)
- Raessi, M., and Mostaghimi, J. (2005). "Three-Dimensional Modeling of Density Variation Due to Phase Change in Complex Free Surface Flows," *Numerical Heat Transfer, Part B: Fundamentals*, **47** (6), pp. 507-531.
[doi:10.1080/10407790590928964](https://doi.org/10.1080/10407790590928964)
- Sicilian, J. M., Hirt, C. W. (1988). "Flow-3D: Computational modeling power for scientists and engineers," Technical Report FSI-88-00-1, *Flow Science Inc.* San Diego, CA.
- Stankus, S. V., and Khairulin, R. A. (2006). "The Density of Alloys of Tin-Lead Systems in the Solid and Liquid States," *High Temperature*, **44** (3), pp.393-400.
[doi:10.1007/s10740-006-0048-5](https://doi.org/10.1007/s10740-006-0048-5)
- Trapaga, G., and Szekely, J. (1991). "Mathematical modeling of the isothermal impingement of liquid droplets in spraying processes," *Metall. Trans.* **B 22**, p 901.
[doi:10.1007/BF02651166](https://doi.org/10.1007/BF02651166)

Trovant, M., and Argyropoulos, S. A. (1996). "Mathematical modeling and experimental measurements of shrinkage in the casting of metals," *Can. Metall. Quart.*, **35**, pp. 77-84.
[doi:10.1016/0008-4433\(95\)00029-1](https://doi.org/10.1016/0008-4433(95)00029-1)

Tsurutani, K., Yao, M., Senda, J., and Fujimoto, H. (1990). "Numerical analysis of the deformation process of a droplet impinging upon a wall," *JSME Int. Ser. II* 33, p 555.

Voller, V. R., and Prakash, C. A. (1987). "Fixed-Grid Numerical Modeling Methodology for Convection-Diffusion Mushy Region Phase-Change Problems," *Int. J. Heat Mass Transfer*, **30**, pp.1709-1720.
[doi:10.1016/0017-9310\(87\)90317-6](https://doi.org/10.1016/0017-9310(87)90317-6)

Waldvogel, J. M., and Poulidakos, D. (1997). "Solidification phenomena in picoleter size solder droplet deposition on a composite substrate," *Int. J. Heat Mass Transfer* **40**, pp. 295-309.
[doi:10.1016/0017-9310\(96\)00107-X](https://doi.org/10.1016/0017-9310(96)00107-X)

Zhao, Z., Poulidakos, D., and Fukai, J. (1996). "Heat transfer and fluid dynamics during the collision of a liquid droplet on a substrate-I, Modeling," *Int. J. Heat Mass transfer* **39**, pp. 2771-2789.
[doi:10.1016/0017-9310\(95\)00305-3](https://doi.org/10.1016/0017-9310(95)00305-3)

Zheng, L. L., and Zhang, H. (2000). "An adaptive level set method for moving-boundary problems: application to droplet spreading and solidification," *Numer. Heat Transfer*, **B 37**, pp. 437-454.
[doi:10.1080/10407790050051137](https://doi.org/10.1080/10407790050051137)